chemistry proceedings

MDPI

Proceeding Paper

Computational Simulation of Supramolecular Interaction Between Tetrodotoxin and Graphene †

Mercedes Álvarez [1,*], Álvaro Antelo [1,*]

[1] Laboratorio CIFGA S.A., Avenida Benigno Rivera, NO.56, 27003 Lugo
* Correspondence: mercedes.alvarez@cifga.com (M.A.); alvaro.antelo@cifga.com (A.A.)
† Presented at the 26th International Electronic Conference on Synthetic Organic Chemistry; Available online: https://ecsoc-26.sciforum.net.

Abstract: In this research, graphene-surface was used as an adsorbent for the evaluation of the supramolecular interaction energies of Tetrodotoxin and molecular analogs using Merck Molecular Force Field (MMFF94). Energy values obtained for Tetrodotoxin supramolecular complexes with graphene sheet and analogs are comparable with values found for the same interaction study for Paralytic shellfish poisoning. All optimized supramolecular complexes lie within an energy window of 2 kcal/mol. The higher adsorption capacity was found by a simulated reduced-GO sheet when comparing the energy of TTX supramolecular complexes. These rGO interaction values from the MMFF94 model result in a better predictive retention time pattern comparing chromatographic elution using a HPLC-Hypercarb column.

Keywords: Tetrodotoxin; graphene; supramolecular; MMFF94

Citation: Álvarez, M.; Antelo, Á. Computational Simulation of Supramolecular Interaction Between Tetrodotoxin and Graphene. **2022**, *4*, x. https://doi.org/10.3390/xxxxx

Academic Editor(s):

Published: 15 November 2022

1. Introduction

Tetrodotoxin (TTX) is a low molecular weight non-proteinaceous potent neurotoxin. TTX has a heterocyclic structure consisting of a guanidinium group and a 2,4-dioxaadamantane skeleton with five hydroxyl moieties (Figure 1). TTX polarity is comparable to saxitoxin despite having only one guanidinium group[1–3].

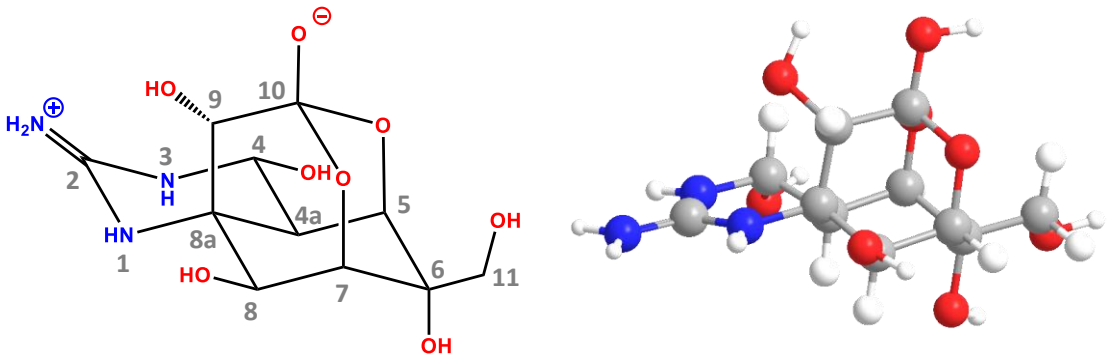

Figure 1. Structure of Tetrodotoxin. (a) atom position, (b) TTX guanidinium-cation ball and stick representation TTX has similar biological activity blocking the voltage-sensitive Na+ channel as STX. Tetrodotoxin and analogs are the active toxins of pufferfish poisoning. The positive guanidinium group is charged at physiological pH and the hydroxyl groups are responsible for binding to the sodium channel (Figure 2)[4].

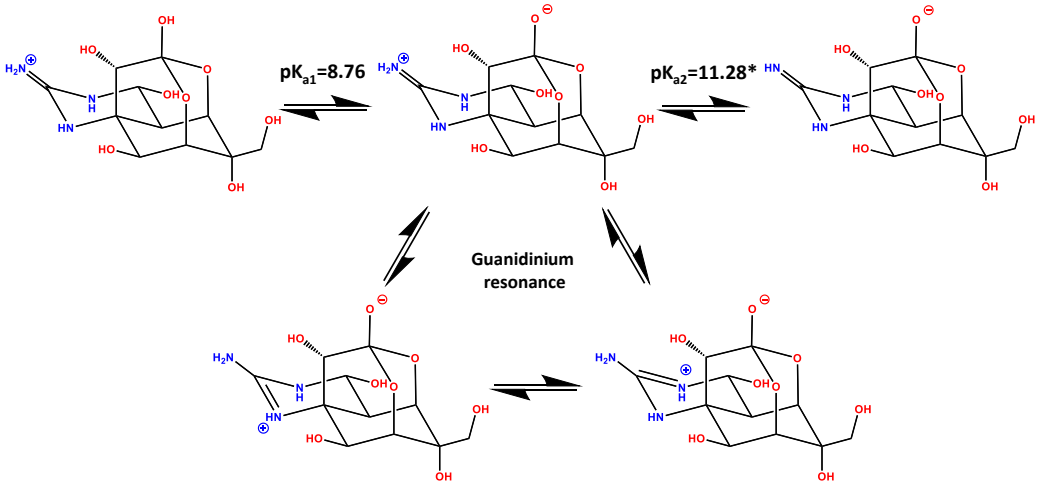

Figure 2. TTX charge state as a function of the respective pK$_a$s values. **pK$_{a1}$ =8.76** for C10-hydroxyl group[5,6]. ***pK$_{a2}$ = 11.28** taken from pk$_a$s from saxitoxin's 1,2,3-guanidinium group[7]. pka of the guanidine in TTX cannot be determined accurately because of decomposition in basic solution[5]. Guanidinium cation structures stabilized by resonance are depicted only for zwitterionic form.

Tetrodotoxin exists as a mixture of hemilactal and lactone forms, Figure 3. TTX NMR analysis from Laboratorio CIFGA S.A. in aqueous [AcOH] = 1 mM, pH = 3.91 reveals an hemilactal and 10,7-lactone ratio around 3.6–4.4 similar to those found in the literature, around 4:1 ratio. The rigidity of the entire skeleton is undoubtedly a factor that favors equilibration with the hemilactal form, resulting in the formation of the dioxaadamantane nucleus[5].

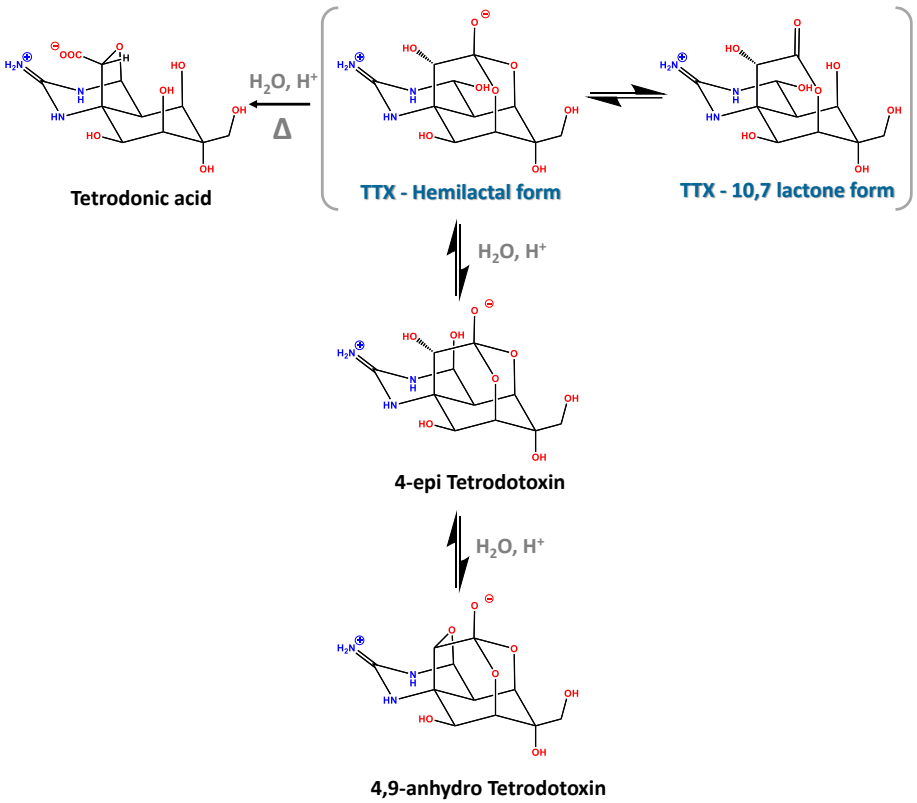

Figure 3. Tetrodotoxin moieties interconversion in aqueous media. Experimental qNMR data at 25ºC in CD3COOD/D2O (4/100, v/v) show a ratio $hemilactal/10{,}7\ lactone \approx 3.6 - 4.4$. Tetrodonic acid is obtained when tetrodotoxin is refluxed in water.

Moreover, TTX also exists as a chemical equilibrium mixture of TTX, 4-epiTTX, and 4,9-anhydroTTX in acidic aqueous solution (Figure 3). Tetrodotoxin turned into 4-epiTTX, and 4,9-anhydroTTX in acidic aqueous solution at 80° C and partially further into tetrodonic acid at 90°C. TTX epimerization yields instability of TTX in solution, this epimerization takes place through special C-4 adjacent to N-3 of the guanidinium group, i.e., 4-Deoxy-tetrodotoxin is very stable as it did not change in a water solution after being boiled for 2 h[8].

There are more than 30 naturally occurring analogs of TTX whose degree of toxicity vary according to structure: number and position of hydroxyl groups present in the structure. TTX and its analogs are widely distributed among marine and terrestrial animals and have the potential to induce dangerous intoxications. Their toxicity varies with structure[9]. It is found that deoxy analogs of TTX are less toxic than TTX, while hydroxyl analogs are more toxic[1]. TTX analogs studied in this research are shown in Figure 4.

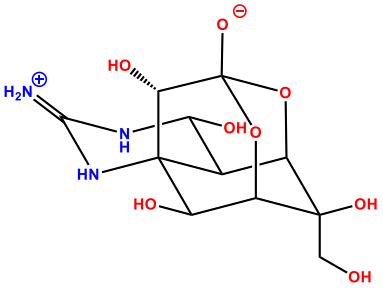

6-epiTTX

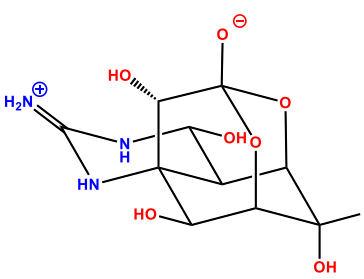

11-deoxyTTX

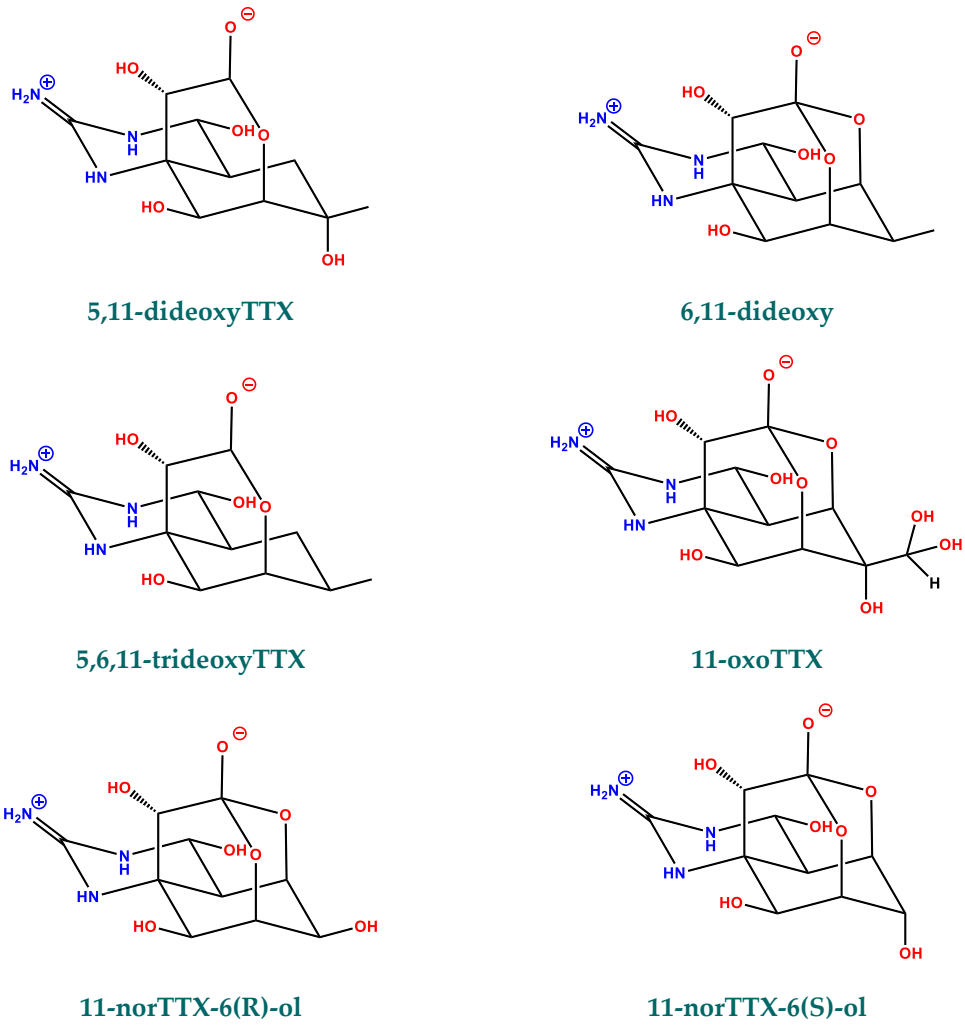

Figure 4. Tetrodotoxin analogs studied in this research.

The counterpart to toxins in this theoretical study is Graphene (G). Graphene, a promising material in the field of nanotechnology, is a nanosheet of sp2-carbon atoms organized in a hexagonal lattice. Graphene-based materials (GBMs) are materials with great potential to be used as a sorbent due to their very large surface area[10,11]. Graphene oxide and reduced graphene oxide are graphene derivatives whose main difference lies in oxygen content:

Graphene oxide (GO): the oxidized form of graphene. The abundance of functional groups results in a hydrophilic behavior strongly dependent on the oxidation level. The C/O ratio is low. Graphene is known to be a hydrophobic material, whereas GO contains nanoscale hydrophilic and hydrophobic domains[12].

Reduced graphene oxide (rGO): reduction of graphene oxide, still contains residual oxygen and structural defects originated. The C/O ratio is higher than GO and also almost zero. The higher the C/O ratio the closer the properties of rGO to the properties of graphene. The rGO monolayer used in this research is obtained by tuning the oxygen content of the graphene framework used for primary calculations, Figure 5.

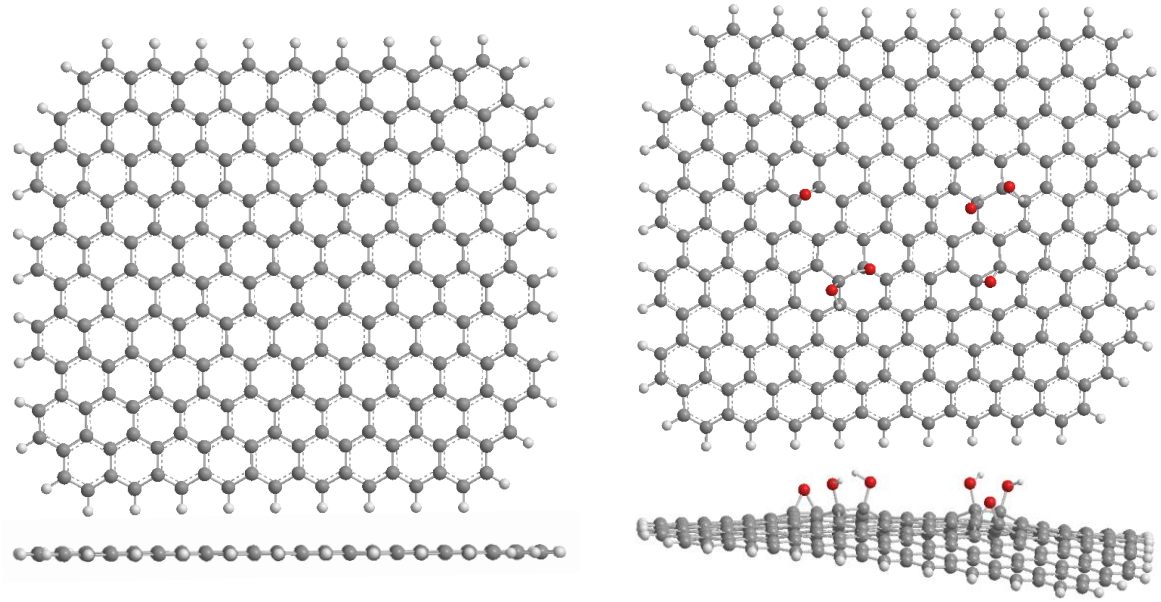

(a) **(b)**

Figure 5. MMFF94 Minimized Chemical 3D frameworks of the Graphene sheet (a) and designed reduced graphene oxide (b) used in this research. Molecular formulas are $C_{234}H_{40}$ and $C_{234}H_{44}O_6$ for Graphene and rGO respectively. rGO is constructed from graphene by hydroxyl and epoxy groups addition. The optimized graphene structure is almost planar while the inclusion of epoxy and hydroxyl groups results in a noticeable curvature for the rGO.

The presence of tetrodotoxin and its analogs in several kinds of matrixes can be determined by several detection methods[13–15]. Recently, we developed a liquid-chromatography method with fluorescence detection or MS/MS to analyze TTX and PSPs in shellfish matrixes. It was based on the use of a porous graphitized column, Hypercarb (Figure 6)[16,17].

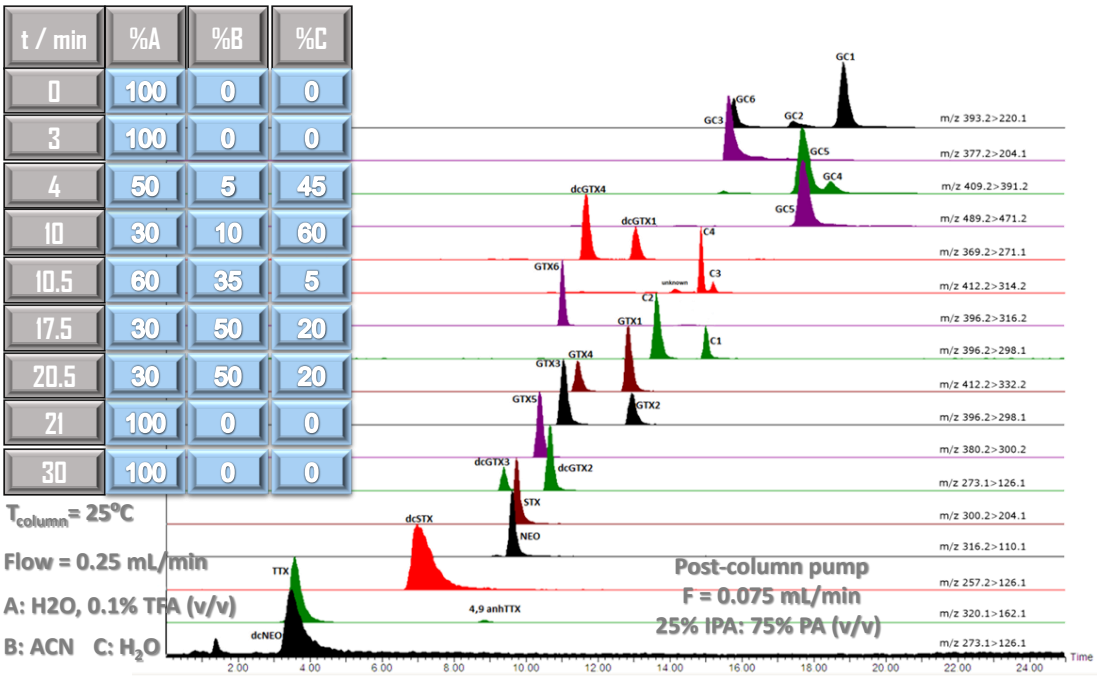

Figure 6. Chromatography of PSPs + TTXs on Hypercarb column.

Commercial TTX purified from pufferfish is typically sold in two forms, with or without citrate buffer. Laboratories under an ISO 17025 accreditation need to validate measurement results are traceable through certified reference materials (CRMs) from a competent producer whose measurements of concentration, uncertainty values, homogeneity and stability studies are clearly stated, namely that are fully metrologically traceable[18].

Certified Reference Material of TTX including a mixture of TTX, 4-epiTTX, and 4,9-anhydroTTX in acidic aqueous solution is supplied by Laboratorio CIFGA S.A. stipulated by ISO 17034:2016[19] accreditation. Certified Reference Material of TTX, CRM-03-TTXs (20-001), presents a 73.9 % (TTX): 20.2 % (4,9-anhydroTTX): 5.9% (4-epiTTX) ratio in aqueous [AcOH] = 1 mM, pH 3.91. Data are similar to the ratio 4:1 for TTX:4,9-anhydroTTX pair (NMR) for the slow equilibrium mixture of TTX and 4,9-anhydroTTX[5].

This batch also contains small amounts of non-certified analogs: tentative 4,4a-anhydro Tetrodotoxin (4,4a-anhTTX), monoformyl Tetrodotoxin (monoformylTTX) and 11-deoxy Tetrodotoxin (11-deoxyTTX) which could be significant to settle retention time of these minority analogs[20].

Commercial TTX Certified Reference Materials are obtained based on a primary quantification using qNMR spectroscopy and a secondary quantification using HILIC-MS/MS. The fact of introducing a different separation methodology, Hypercarb, allows presenting a better characterization of the impurities in the certificates. Both CRM-03-TTXs batches 12-001 (obsolete) and 20-001 (updated) present: TTX, 4-epiTTX, and 4,9-anhydro-TTX by equilibrating tetrodotoxin in aqueous solution and re-analyzed by HPLC-MS/MS on Hypecarb column, Figure 7.

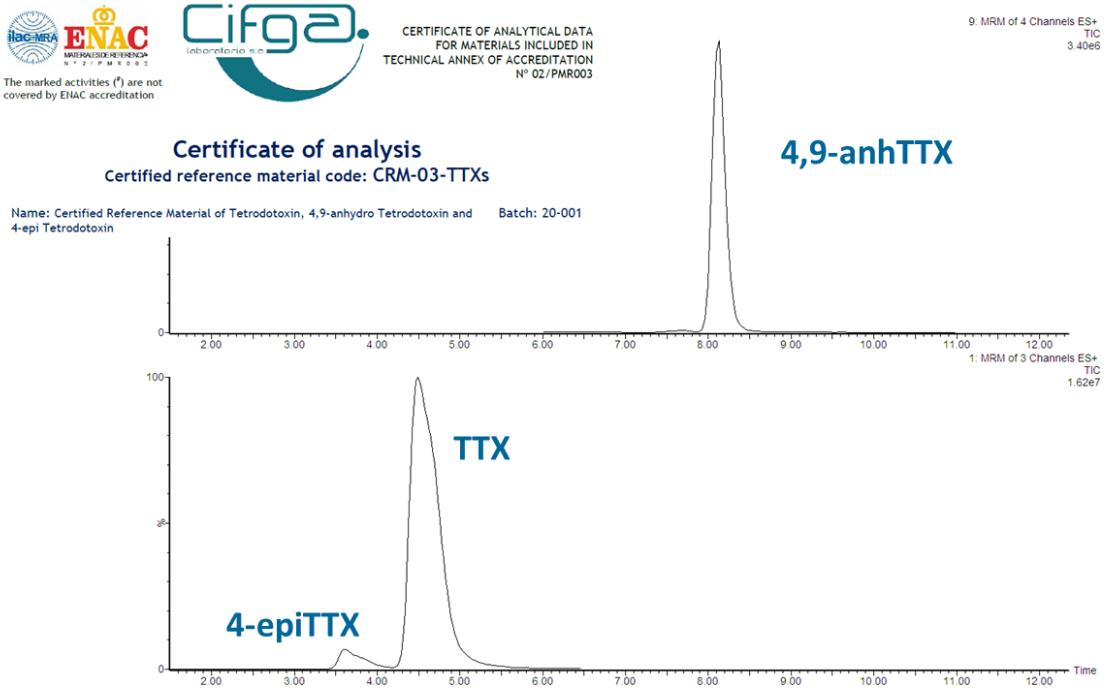

Figure 7. Chromatography of CRM-03-TTXs (20-001) on Hypercarb column. Chromatographic method of Figure 6. The obsolete batch 12-001 contained traces of four analogs: 11-deoxyTTX, 4-epiTTX, 5,6,11-trideoxyTTX and norTTX. Meanwhile the updated batch 20-001 contains: tentative 4,4a-anhydro Tetrodotoxin (4,4a-anhTTX), monoformyl Tetrodotoxin (monoformylTTX) and 11-deoxy Tetrodotoxin (11-deoxyTTX) as impurities.

2. Objectives

The purpose of this molecular simulation is to understand the supramolecular interaction mechanism of TTXs over a graphene surface through a molecular mechanics force

field (MMFF94) and to calculate the strength of the supramolecular process of toxin/graphene through the energy of molecular self-assembly.

3. Methodology

To help the understanding of the mechanism of supramolecular interaction of TTXs with graphene surface, computational simulation of the single molecules and final supramolecular structures was performed using the Merck Molecular Force Field 94 (MMFF94) implemented in Chem3D version 18.1[21,22].

As in our previous work, the procedure involves the following steps:

(1) The 2D structures of all the compounds were constructed in the builder module of ChemDraw software. The 2D structures of the compounds were transferred to Chem3D.

(2) The conformations were optimized using Merck Molecular Force Field 94 (MMFF94). Geometry optimizations for all molecules were computed using convergence criteria for root-mean-square for the gradient of the potential energy surface of 0.001 kcal/mol. No essential difference was observed if 0.002 kcal/mol is used as convergence criteria. E_{toxin} is the potential energy of the toxin (adsorbate) and $E_{graphene}$ is the potential energy of graphene (substrate).

(3) A bottom-up scheme, in which the starting topology consists of a toxin placed at the center of the graphene sheet (234 carbon atoms, $C_{234}H_{40}$) separated by approximately 5-6 Amstrongs. Then the energy and geometry of the supramolecular complex were optimized, without fixing the position of the graphene atoms in space to obtain $E_{supramolecular}$ (potential energy of the complex in vacuum at the local minimum).

(4) The calculations were made in an Intel Dual Core 2.6 GHz computer with 8 Gb of RAM. Computational analysis of liquid chromatography retention was carried out taking into account the following approximations:

1. Minimizations were performed without solvents (vacuum is the media of minimizations).

2. Final supramolecular complex is a local minimum energy, to get a value to can make a statistical energy suggestion, taking into account 0.15 kcal/mol was the difference between the minimum planar conformation energy of graphene and the energy of the sheet after the interaction that can be used as the minimum value to assess the absorption energy. We should notice that small molecule minimization results depend on initial conformation and internal hydrogen bonding. Problems with possible biases due to TTX intramolecular hydrogen bonding can be included in a 0.19 kcal/mol energy factor, Figure 8. Total ±0.34 kcal/mol is the minimum potential energy which is taken as energy error to differentiate two local minimum conformers.

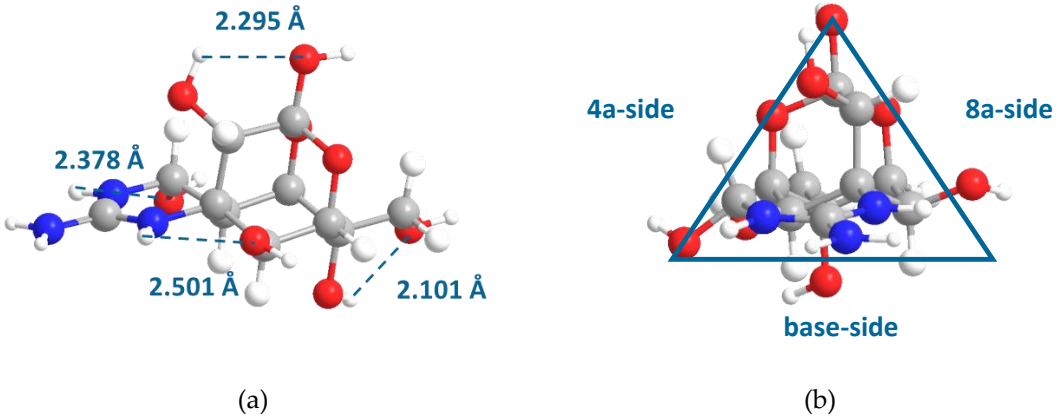

Figure 8. (a) Distance of tentative intramolecular hydrogen bonding in TTX cationic form. (b) Stereostructure of tetrodotoxin with our triangular side nomenclature to define three-dimensional interaction with graphene. Different orientations of the molecule can affect the binding energy.

3. Tetrodotoxin is often chemically represented as a zwitterion. Since the pka of C10 hemilactal is 8.76 therefore Tetrodotoxin is found in the cationic form at lower pH values. In this research, we only evaluate the interaction with this form. For convenience, a new approach where the guanidinium group with the charge located in the $(C = N_2^+)$ group is studied instead of evaluating the three resonance forms.

4. The topology of the initial toxin alignment is crucial to the value of this method. Tetrodotoxin interaction with graphene is evaluated by comparing three different approaches: from a nearly flat side where the carbon-4a is located, one with the carbon-8a carbon and one as the base of the dioxaadamantane group, Figure 6b.

5. The binding energy of single toxins (with and without counter anion) adsorbed on a large poly-aromatic hydrocarbon mimicking graphene substrate was determined by subtracting the energy of the toxin and the graphene model from that of the supramolecular complex.

$$\Delta E = E_{supramolecular} - (E_{toxin} + E_{graphene}) \quad (1)$$

Where $E_{supramolecular}$ is the potential energy of the complex in vacuum at the minimum, and E_{toxin} and $E_{graphene}$ the potential energies of the adsorbate and the substrate separated at an infinite distance.

4. Results and Discussion

Toxin adsorption over graphene were evaluated without counter anions, taking into account only the guanidinium-cationic $(C = N_2^+)$ conformation. The corresponding energy values are shown in Table 1

Table 1. Energy values of TTXs and supramolecular complexes with graphene sheet, without counter-anion. Values are given in kcal/mol.

Molecule	Approachment	$E_{molecule}$	ΔE
Graphene	-	1200.825	
TTX-hemiacetal	Base-side		-24.29
TTX-hemiacetal	4a-side	-157.548	-22.68
TTX-hemiacetal	8a-side		-21.63
TTX-10,7-lactone	Base-side	-105.007	-24.73
4-epiTTX	Base-side	-152.609	-24.19
4,9-anhydroTTX	Base-side	-145.316	-24.60
6-epiTTX	Base-side	-149.845	-24.12
11-deoxyTTX	Base-side	-169.259	-23.97
5,11-dideoxyTTX	Base-side	-135.725	-24.37
6,11-dideoxyTTX	Base-side	-202.705	-25.06
5,6,11-trideoxyTTX	Base-side	-148.288	-25.35
11-oxoTTX	Base-side	-175.980	-24.26
11-nor-TTX-6(R)-ol	Base-side	-174.693	-24.22
11-nor-TTX-6(S)-ol	Base-side	-176.222	-23.66

When TTX is adsorbed on the graphene, Tetrodotoxin gradually approaches the surface and the graphene slightly moves from the planar configuration. Two approaching stages were observed before a local minimum equilibrium structure was reached. In a first stage, the noncovalent cation–π force is responsible for the approach, while in a second stage the stabilization can be associated with the presence of CH···π interactions. After around 6000–12000 steps, an equilibrium structure is reached.

TTX minimum structure 3D model shows a quasi-planar interaction between each of the triangular sides with a graphene layer, an average plane of van der Waals contact atoms around 2.9–3.1 Å, Figure 9. It must be noted that guanidinium contact with the

surface is approximately about 3.0 amstrongs, similar values to the guanidium group from PSTs[23].

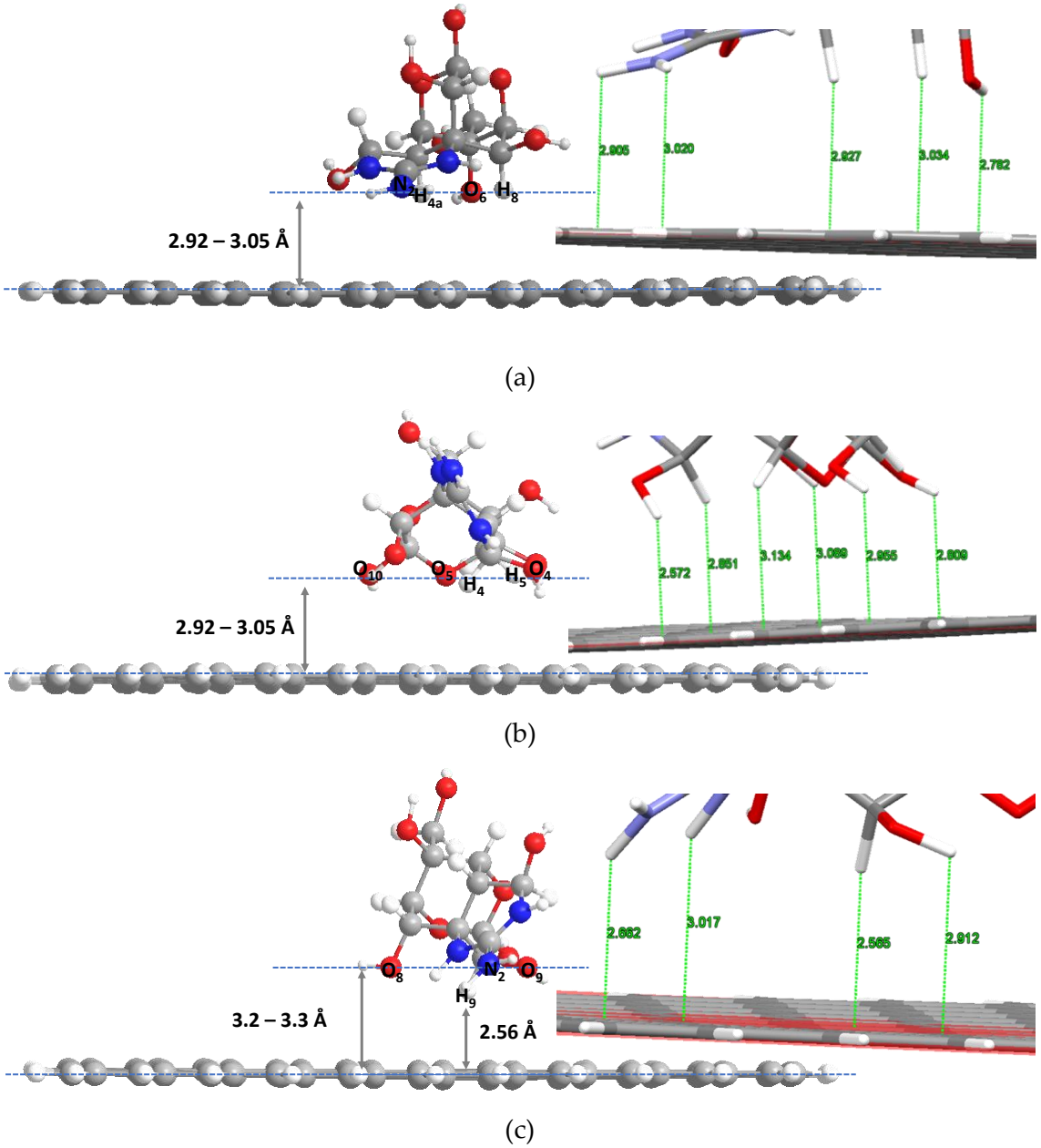

Figure 9. 3D model of the local optimized geometry for the basal plane of graphene with TTX: (a) Dioxadamantane base-side. (b) 4a-side. (c) 8a-side orientations. Distances were calculated using Mercury software[24].

Dioxadamantane base-side approximation is the most favorable. Cation–π through two hydrogens of iminium group, two CH–π and one polar–π close contacts (van der Waals plane) yield less energetic conformation than base-4a approaching which presents six contacts through two CH–π and four polar–π interactions. In this local minimum no cation–π alignment was reached. Base-8a approximation takes place by H of the iminium group, one CH group and one hydroxyl group.

Tetrodotoxin in solution exists as an equilibrium mixture of its ortho ester, lactone, anhydride and epi forms, the set of generated target interaction energies agree fairly well being 10,7 lactone is the most favorable moiety, although the energetic value is similar to 4,9-anhydroTTX (fall inside ±0.34 kcal/mol).

The most stable supramolecular complexes take place in 6,11-dideoxyTTX and 5,6,11-trideoxyTTX. The lack of the hydroxyl group in the axial position at C6 is the main factor. If we analyze the epimeric pair 11-nor-TTX-6(R)-ol versus 11-nor-TTX-6(S)-ol we find the same result. Graphene interaction with H-alkane is preferred instead of the hydroxyl group. The lack of 6-axial-hydroxyl induces a closer approximation of a plane formed H8-H4-H6 axial protons of adamantane base to graphene surface at the cost of slightly increasing the cation–π distance. Therefore, the closer adamantane-base van der Waals interaction with graphene supports adsorption despite increasing space for non-covalent bonding between a monopole (cation) and a quadrupole (π system), Figure 10.

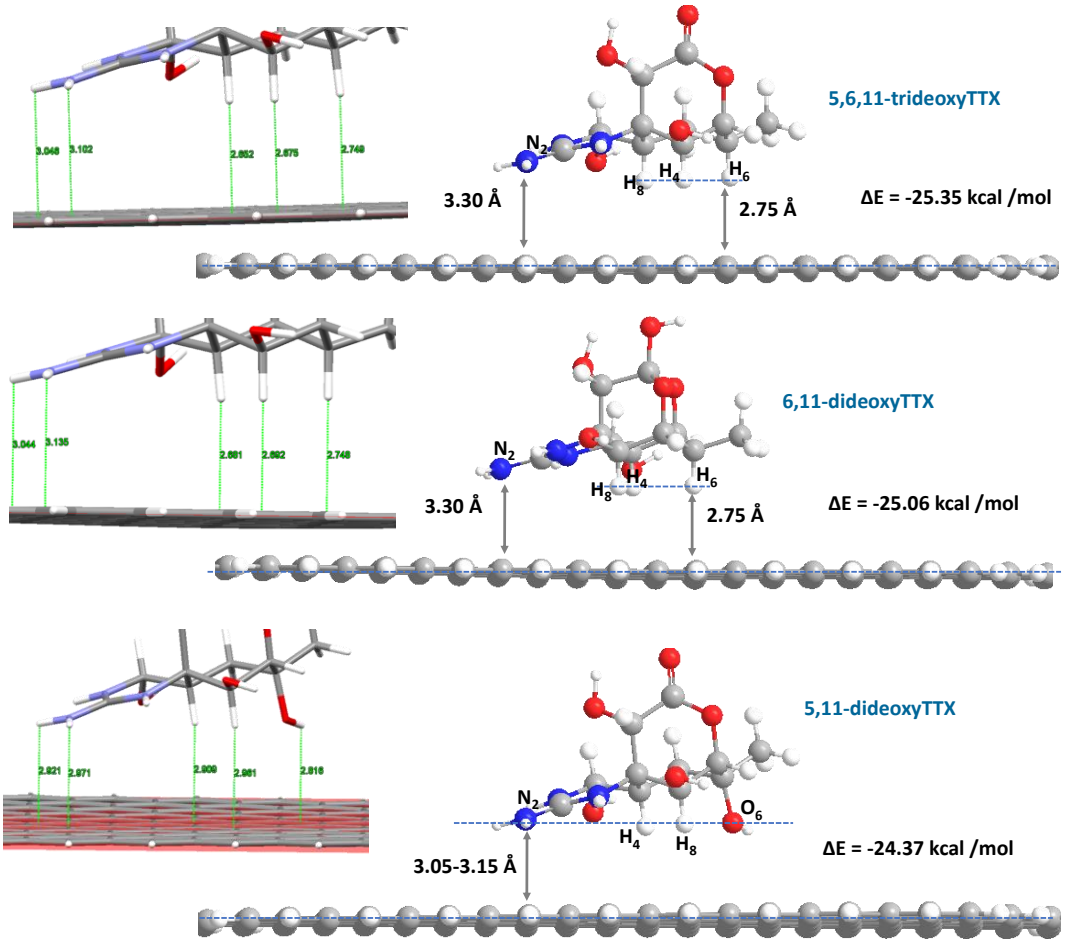

Figure 10. 3D model of minimum energy of supramolecular complex of graphene layer with 5,6,11-trideoxyTTX, 6,11-dideoxyTTX and 5,11-dideoxyTTX through dioxadamantane base-side approximation.

Hypercarb column, porous graphite carbon, is used to separate different analogs of TTX and PSPs, Figure 7. The elution order for TTXs is 4epiTTX–TTX–4,9-anhTTX, according to values of Table 1 theoretical elution order is screened by a statistical value of 0.34 kcal/mol due to local minimum energy conformations.

Table 2 shows the same results but includes TFA as a counter-anion to the system. TFA is an additive used in the mobile phase for TTX elution. But the same problem is encountered to establish a theoretical elution order at lower energy values because the TFA interacts with the guanidinium residues and the charges will be screened to remain available for the interaction with the surface, therefore cation-π interaction is reduced.

The mobile phase is a major determinant of retention because it influences the ionization state of both analytes and the PGC surface. Trifluoroacetic acid and water could modify the oxidation state of the graphite surface. rGO possesses the ability to form

hydrogen bonds with the neighboring molecules, no such interactions can take place at the surface of graphene. According to a higher oxidation state of graphite, a simulated rGO is used to evaluate TTX interaction. Energy values for some analogs are shown in Table 3.

Table 2. Energy values of TTXs using TFA as a counterion and supramolecular complexes with a graphene sheet. Values are given in kcal/mol.

Molecule	Approximation	E[illegible]	ΔE
Graphene	-	1200.825	
TTX-hemiacetal	Base-side	-117.899	-19.44
TTX-10,7-lactone	Base-side	--68.177	-19.86
4-epiTTX	Base-side	-105.848	-19.68
4,9-anhydroTTX	Base-side	-107.974	-19.62
6-epiTTX	Base-side	-113.672	-18.73
11-deoxyTTX	Base-side	-129.342	-18.89
5,11-dideoxyTTX	Base-side	-99.945	-19.50
6,11-dideoxyTTX	Base-side	-164.944	-20.92
5,6,11-trideoxyTTX	Base-side	-114.912	-21.00
11-oxoTTX	Base-side	-135.797	-19.14
11-nor-TTX-6(R)-ol	Base-side	-139.350	-19.34
11-nor-TTX-6(S)-ol	Base-side	-136.495	-20.26

In silico characterization of TTX and rGO yields lower energy values for the supramolecular complexes. Thus, the interaction between each analog and rGO 2D sheet is likely to be the most effective. The adsorption energy values now better match the retention time values: 4epiTTX–TTX–4,9-anhTTX.

Table 3. Energy values of TTXs without TFA as a counterion and supramolecular complexes with rGO sheet. Values are given in kcal/mol.

Molecule	Approximation	E[illegible]	ΔE
rGO	-	1304.808	
TTX-hemiacetal	Base-side	-157.548	-52.12
4-epiTTX	Base-side	-152.609	-49.72
4,9-anhydroTTX	Base-side	-145.316	-53.26
5,6,11-trideoxyTTX	Base-side	-148.288	-54.24

The introduction of hydroxyl and epoxy groups on the surface of graphene leads to hydrogen bonding between the adsorbent and the substrate, Figure 11.

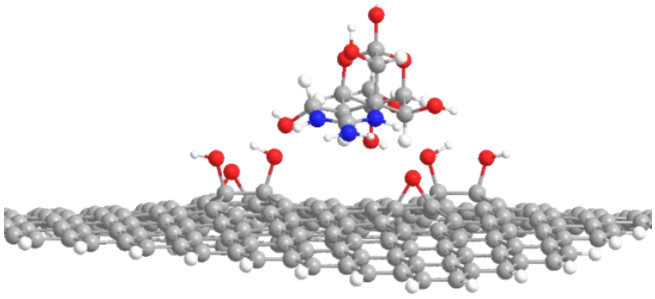

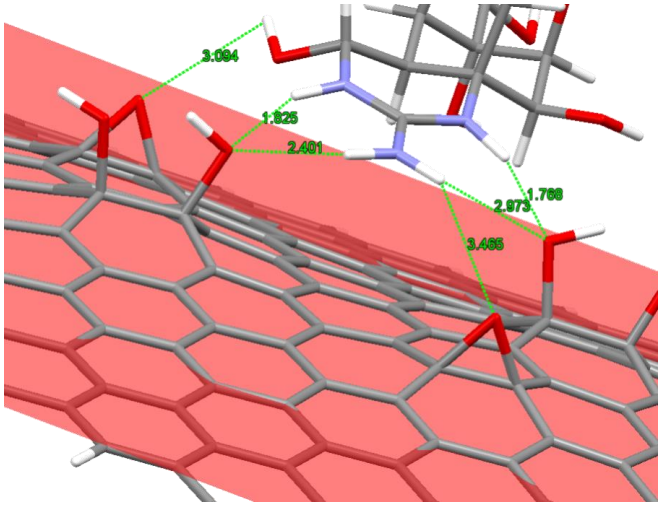

Figure 11. 3D model of minimum energy of supramolecular complex of rGO layer with TTX through dioxadamantane base-side approximation.

5. Conclusions

In conclusion, we have studied the interaction of TTXs with graphene theoretically. The dominant forces during the adsorption are mainly cation–π and hydrophobic interactions than hydrophilic (polar–π).

Due to structural differences each toxin has a slightly different affinity to the graphene surface but, small variations of the computational energy values do not show a specific correlation with the experimental elution order of TTX, 4,9-anhTTX, and 4-epiTTX found on chromatography over PGC column.

Tuning graphene, modifying the oxidation state, yields a better approach to experimental adsorption by introducing hydrogen bonding interactions between the adsorbent and substrate. This work could help to understand better the nature of the interactions between TTX and analogs with graphene and contribute to the design of new materials to improve the removal and analysis of this family of molecules. This approach may also be useful to predict interactions in other possible applications such as chromatographic molecular separations.

References

(1) Bane, V.; Lehane, M.; Dikshit, M.; O'Riordan, A.; Furey, A. Tetrodotoxin: Chemistry, Toxicity, Source, Distribution and Detection. *Toxins* **2014**, *6* (2), 693–755. https://doi.org/10.3390/toxins6020693.

(2) Tsuda, K.; Ikuma, S.; Kawamura, M.; Tachikawa, R.; Sakai, K. Tetrodotoxin. VII. On the Structure of Tetrodotoxin and Its Derivatives. *Chem. Pharm. Bull. (Tokyo)* **1964**, *12* (11), 1357–1374. https://doi.org/10.1248/cpb.12.1357.

(3) Woodward, R.B.; Gougoutas, J. Zanos. The Structure of Tetrodotoxin. *J. Am. Chem. Soc.* **1964**, *86* (22), 5030–5030. https://doi.org/10.1021/ja01076a076.

(4) Fozzard, H.A.; Lipkind, G. The Guanidinium Toxin Binding Site on the Sodium Channel. *Jpn. Heart J.* **1996**, *37* (5), 683–692. https://doi.org/10.1536/ihj.37.683.

(5) Goto, T.; Kishi, Y.; Takahashi, S.; Hirata, Y. Tetrodotoxin. *Tetrahedron* **1965**, *21* (8), 2059–2088. https://doi.org/10.1016/s0040-4020(01)98344-9.

(6) Roggatz, C.C.; Fletcher, N.; Benoit, D.M.; Algar, A.C.; Doroff, A.; Wright, B.; Wollenberg Valero, K.C.; Hardege, J.D. Saxitoxin and Tetrodotoxin Bioavailability Increases in Future Oceans. *Nat. Clim. Change* **2019**, *9* (11), 840–844. https://doi.org/10.1038/s41558-019-0589-3.

(7) Rogers, R.S.; Rapoport, H. The PKa's of Saxitoxin. *J. Am. Chem. Soc.* **1980**, *102* (24), 7335–7339. https://doi.org/10.1021/ja00544a030.

(8) Lin, W.; Huang, X.; Zhang, X. Stable Pharmaceutical Composition of Freeze-Dried Tetrodotoxin Powder. US8530481B2, September 10, 2013.

(9) Yotsu-Yamashita, M.; Sugimoto, A.; Takai, A.; Yasumoto, T. Effects of Specific Modifications of Several Hydroxyls of Tetrodotoxin on Its Affinity to Rat Brain Membrane. *J. Pharmacol. Exp. Ther.* **1999**, *289* (3), 1688–1696.

(10) Maciel, E.V.S.; Mejía-Carmona, K.; Jordan-Sinisterra, M.; da Silva, L.F.; Vargas Medina, D.A.; Lanças, F.M. The Current Role of Graphene-Based Nanomaterials in the Sample Preparation Arena. *Front. Chem.* **2020**, *8*, 664. https://doi.org/10.3389/fchem.2020.00664.

(11) Bhol, P.; Yadav, S.; Altaee, A.; Saxena, M.; Misra, P.K.; Samal, A.K. Graphene-Based Membranes for Water and Wastewater Treatment: A Review. *ACS Appl. Nano Mater.* **2021**, *4* (4), 3274–3293. https://doi.org/10.1021/acsanm.0c03439.
(12) Hampitak, P.; Melendrez, D.; Iliut, M.; Fresquet, M.; Parsons, N.; Spencer, B.; Jowitt, T.A.; Vijayaraghavan, A. Protein Interactions and Conformations on Graphene-Based Materials Mapped Using a Quartz-Crystal Microbalance with Dissipation Monitoring (QCM-D). *Carbon* **2020**, *165*, 317–327. https://doi.org/10.1016/j.carbon.2020.04.093.
(13) Katikou, P.; Vlamis, A. Tetrodotoxins: Recent Advances in Analysis Methods and Prevalence in European Waters. *Curr. Opin. Food Sci.* **2017**, *18*, 1–6. https://doi.org/10.1016/j.cofs.2017.09.005.
(14) Turner, A.D.; Boundy, M.J.; Rapkova, M.D. Development and Single-Laboratory Validation of a Liquid Chromatography Tandem Mass Spectrometry Method for Quantitation of Tetrodotoxin in Mussels and Oysters. *J. AOAC Int.* **2017**, *100* (5), 1469–1482. https://doi.org/10.5740/jaoacint.17-0017.
(15) Hu, C.; Zhang, Y.; Zhou, Y.; Xiang, Y.; Liu, Z.; Wang, Z.; Feng, X. Tetrodotoxin and Its Analogues in Food: Recent Updates on Sample Preparation and Analytical Methods Since 2012. *J. Agric. Food Chem.* **2022**, *70* (39), 12249–12269. https://doi.org/10.1021/acs.jafc.2c04106.
(16) Rey, V.; Botana, A.M.; Alvarez, M.; Antelo, A.; Botana, L.M. Liquid Chromatography with a Fluorimetric Detection Method for Analysis of Paralytic Shellfish Toxins and Tetrodotoxin Based on a Porous Graphitic Carbon Column. *Toxins* **2016**, *8* (7), 196. https://doi.org/10.3390/toxins8070196.
(17) Rey, V.; Botana, A.M.; Antelo, A.; Alvarez, M.; Botana, L.M. Rapid Analysis of Paralytic Shellfish Toxins and Tetrodotoxins by Liquid Chromatography-Tandem Mass Spectrometry Using a Porous Graphitic Carbon Column. *Food Chem.* **2018**, *269*, 166–172. https://doi.org/10.1016/j.foodchem.2018.07.008.
(18) ISO/IEC 17025:2017. General Requirements for the Competence of Testing and Calibration Laboratories.
(19) ISO 17034:2016. General Requirements for the Competence of Reference Material Producers.
(20) *Cifga Laboratory: Certified reference material producer*. CIFGA. https://cifga.com/ (accessed 2022-10-12).
(21) Perkin Elmer. Chem 3D Ultra. 18.1.
(22) Halgren, T.A. Merck Molecular Force Field. I. Basis, Form, Scope, Parameterization, and Performance of MMFF94. *J. Comput. Chem.* **1996**, *17* (5–6), 490–519. https://doi.org/10.1002/(SICI)1096-987X(199604)17:5/6<490::AID-JCC1>3.0.CO;2-P.
(23) Antelo, Á.; Rey, V.; Álvarez, M.; Botana, A.; Botana, L. Computational Model of Adsorption for Paralytic Shellfish Poisoning Toxins (PSTs) on Graphene Surface. **2016**. https://doi.org/10.3390/ecsoc-20-e006.
(24) Mercury 3.8. Http://Www.Ccdc.Cam.Ac.Uk/Mercury/.

.